SCA2003-27: THE SCALING OF SURFACE-TO-PORE-VOLUME RATIO ESTIMATES AND ITS USE IN PREDICTING NMR LOG DERIVED PERMEABILITIES IN CLASTIC ROCKS. MODEL DRIVEN FIELD APPLICATIONS FROM THE LUBLIN BASIN, POLAND

Hendrik Rohler, RWE Dea AG, Hamburg, Germany

This paper was prepared for presentation at the International Symposium of the Society of Core Analysts held in Pau, France, 21-24 September 2003

ABSTRACT

The permeability of clastic materials is controlled by the solid-void distribution function (SVDF). Different studies show that it may suffice to relate permeability to functions of lower order moments of the SVDF, namely porosity, tortuosity, and specific inner surface area. Direct as well as indirect lab methods for measuring surface areas are based on physical processes operating on characteristic length scales. Therefore recipes for matching them on the hydraulic permeability scale, equivalent to the Kozeny-Carman hydraulic capillary radius, are needed. This paper shows the strong correlation between surface area estimates derived from nitrogen gas adsorption (BET), mercury intrusion capillary pressure (MICP), and transverse nuclear magnetic resonance measurements (TNMR) on vintage core plugs of Permian and Carboniferous age from the Lublin Basin, Poland. The physical significance of these correlations is facilitated by comparing results to a fractal void-solid interface model, the Pape pigeon hole model. The pigeon hole model leads to matched scale expressions for the hydraulic permeability, namely the Paris equation for BET, and a variant of the Kozeny-Carman equation for MICP measurements. Using the Lublin Basin dataset, we show the validity of the Paris permeability equation, demonstrate the scale equivalence of MICP and TNMR inner surface estimates, and derive the Kozeny-Carman equation for TNMR data. This latter expression forms the basis for further permeability predictions from TNMR logging tools. For field applications the TNMR permeability estimator is compared with logging expressions derived by Sen and Timur-Coates. Simple multiplier rules are found to match their estimators for clean sands, and a calibrated TNMR log permeability may be arrived at. Finally, two field examples are presented to assess the limits of validity of the approach adopted in this paper and to underline the need for conditional core sampling as suggested by Worthington. We present a case of heuristic equivalence of properly calibrated TNMR permeability log readings with values derived from log data inversion based on Herron's k-lambda method over uncored well sections. In a counter-example the illitisation of pore throats is not captured by the TNMR log as confirmed by comparing with wireline pretest data, sonic derived mobilities, and subsequent sidewall core analyses.

INTRODUCTION

As no single continuous logging tool is able to measure permeability in a direct fashion various interpretation techniques have been devised in the past that rely on inverting logs that respond to varying degree to variations of the specific inner surface area of the logged porous formation, i.e. spontaneous potential, resistivity, sonic slowness and attenuation, and spectral gamma ray logs. These approaches are based on the observation drawn from lab measurements that permeabilities of clastic porous rocks in general are strongly correlated to the lower moments of the SVDF, namely porosity, tortuosity, and surface-to-pore-volume ratio. Presuming applicability of a capillary bundle model this correlation may be cast in the general form of the Kozeny-Carman equation

$$K \cdot F = \frac{1}{8} r_{eff}^2 = \frac{1}{2} S_{por}^{-2} \tag{1}$$

with permeability K measured in Darcy, effective hydraulic radius r_{eff} in um, and hydraulic inner surface area S_{por} in um^{-1}. Basan et.al. [1] give an account relating pore-size data derived from lab based MICP, TNMR, and backscattered electron images (BSEI) to permeability on a vast North Sea dataset. East [2] works lab examples from Australia to relate surface-to-pore-volume ratios using polar molecule adsorption techniques to irreducible water saturation, formation factor, cation exchange capacity, and permeability. More recently Volokitin et.al. [3] published on recipes for computing capillary pressure curves from TNMR spectra. Their vast database revealed a close correlation between irreducible water saturation and log-mean TNMR relaxation rate, a fact they related to the self-similar pore structure.

This paper continues on the path prepared by those authors and stresses the need for obtaining inner surface area data on reservoir core plugs in order to derive reliable permeability estimates. We extend their ideas by incorporating a structural pore model, the pigeon hole model of Pape et.al. [4][5]. With the aid of this model we will be able to convert surface areas derived from measurements of different resolution power. The pigeon hole model leads to matched scale expressions for the hydraulic permeability, namely the Paris equation for BET, and a variant of the Kozeny-Carman equation for MICP measurements. Using the Lublin Basin dataset, we show the validity of the Paris permeability equation, demonstrate the scale equivalence of MICP and TNMR inner surface estimates, and derive the Kozeny-Carman equation for TNMR data. This latter expression forms the basis for further permeability predictions from TNMR logging tools.

As the Lublin Basin database contains only some 50 plugs across similar lithologies from four wells with surface area measurements statistically significant correlations may not be obtained. The use of the structural pigeon hole model then may allow for a secondary statistics approach by comparing data trends to established relations.

The next sections will introduce the relevant equations for converting inner surface areas from MICP and BET measurements based on the pigeon hole model. It will be shown that

strong correlations exist between surface area estimates derived from nitrogen gas adsorption, mercury intrusion capillary pressure, and transverse nuclear magnetic resonance measurements on those core plugs examined.

STRUCTURAL PORE MODEL

The specific inner surface area is a fractal quantity and thus its actual value depends on the power of resolution of the physical method involved in its measurement. The hydraulic surface S_{por} as determined from permeability measurements having a resolution length of r_{eff} given by (1) may be orders of magnitude lower than the BET surface measured by nitrogen gas adsorption [6] having resolution length of the nitrogen molecule diameter d_{N2}. Permeabilties derived from (1) with BET surface values inserted may yield values too low as compared to measured Klinkenberg corrected gas permeabilities. The pigeon hole model provides a quantitative way of converting length scales by representing the pore space as smooth first order hydraulic capillaries superimposed by subsequently smaller self-similar pigeon hole structures (fig.1). For these simple geometrical structures (of model default specific surface fractal Hausdorff dimension D_f of 2.3566) the conversion factor Q_{ik} between S_{por} and $S_{por,BET}$ can be derived where the two different measurement yardsticks enter [5]

$$\log Q_{ik} = \log \frac{S_{por,BET}}{S_{por}} = 0.3566 \log r_{eff} + 0.8507 + \log q_0 \tag{2}$$

with $D_f - 2 = 0.3566$ from the default pigeon hole model, S_{por} and $S_{por,BET}$ measured in um^{-1}, and r_{eff} in um. The lamellar factor q_0 equals one for perfect fractals, $q_0>1$ accounts for lamellar surface enlargements (authigenic clay coatings) and $q_0<1$ for smoothing of the pigeon-hole surface (quartz or carbonate cements). Solving (2) for r_{eff} and inserting into (1) leads to the PARIS equation

$$K \cdot F = 475.33 \left(\frac{S_{por,BET}}{q_0} \right)^{-3.1085} \tag{3}$$

Measured permeability values were cross-plotted with BET surface data to check the applicability of the PARIS equation (fig.2). Most data points fit (3) for lamellar factors ranging from 1 to 2. Both, petrographic analyses by BSEI inspection and XRD measurements qualitatively confirm the range of the lamellar factor. BSEI image data show low contents of pore-lining clay within these samples and the XRD data indicate that only samples with clay contents greater 9 wt.% substantially deviate from the $q_0=1$ and $q_0=2$ trend lines (fig.3).

CONVERSION OF MICP TO BET SPECIFIC SURFACE AREA

The following section expands on the hydraulic yardstick r_{eff} as determined from permeability and formation factor measurements. For the datasets used in deriving the

pigeon hole model [7] and for the Lublin database r_{eff} never gained values below 50nm which correspond to MICP values not exceeding 150 bar, as derived from (5) below. Therefore, from the perspective of the pigeon hole model, P_c data exceeding 150 bar will represent grain surface roughness and clay mineral related dead end pores which are hydraulically inactive pore structures.

Assuming capillary models to be valid descriptors, the specific surface area S_{por} may be calculated from radii distributions derived from primary drainage MICP,

$$S_{por,MICP} = \frac{1}{\Sigma_{Hg,\max}} \int_0^{\Sigma_{Hg,\max}} \frac{2}{r_c\left(\Sigma_{Hg}\right)} \cdot d\Sigma_{Hg} \tag{4}$$

with Σ_{Hg} mercury saturation, and capillary radius r_c derived from the Washburn equation

$$P_c = -\frac{2s \cdot \cos q}{r_c} \tag{5}$$

with σ_{Hg}=0.480Nm^{-1}, θ_{Hg}=140° at standard conditions.

Validity of the MICP-BET correlation was then confirmed by converting $S_{por,MICP}$ values obtained from MICP by means of (4) through use of the appropriate pigeon-hole surface scaling relation [5]

$$\log Q_{ik} = \log \frac{S_{por,BET}}{S_{por,MICP}} = 0.3566 \log r_{\min} + 1.3295 \tag{6}$$

with r_{min} measured in um corresponding to the maximum capillary pressure by (5), and $S_{por,BET}$ and $S_{por,MICP}$ in um^{-1}. First, as suspected, $S_{por,MICP}$ values were smaller than those derived from BET measurements. In a second step the conversion factor Q_{ik} for the pure fractal pigeon-hole model (6) is used which transforms $S_{por,MICP}$ values into order of magnitude of the corresponding $S_{por,BET}$ values. Then the structural parameter q_0 is additionally taken into account. The q_0 values were calculated from permeability measurements according to (2). Figure 4 displays the result of the surface area conversion which now plots slightly above a linear relation. If one disregards data points from samples with high capillary entry pressure and high residual wetting fluid saturations (fig.5) which correspond to samples with XRD clay content above 9 wt.% the resulting conversion then plots slightly below linear. Based on this data we propose the following linear relation to be valid for the Lublin dataset

$$S_{por,MICP} \cdot Q_{ik} \cdot q_0 = 2.5 \cdot S_{por,BET} \tag{7}$$

This line plots above the diagonal, indicating that $S_{por,MICP}$ values obtained from (4) slightly overestimate the effective hydraulic radius to be used in the Kozeny-Carman relation (1).

CORRELATON OF TNMR AND BET SPECIFIC SURFACE AREAS

T1 and T2 measurements on fully water saturated samples were obtained with a MARAN 30 spectrometer. T1 data were sampled using the inversion recovery sequence. T2 data were obtained using a CPMG sequence with inter-echo spacing TE=60us. A reference dataset with TE=200us was obtained on a sample subset to confirm that diffusion is a minor factor to the T2 distribution. When plotting the log-mean T2 relaxation times against $S_{por,BET}$ (fig.6) the resulting correlation is very close to the one predicted by the pigeon-hole model if one assumes that $S_{por,MICP}$ and TNMR derived surface values are measured with a similar yardstick [1]. The scatter of the data points around the correlation line depicted in figure 6, which corresponds to the non-normalized scaling relation

$$\log \tilde{Q}_{ik} = \log\left(S_{por,BET} \cdot T_{2,LM}\right) = 0.3566 \log T_{2,LM} + 0.1734 , \quad (8)$$

may then be attributed to the variance of the surface relaxivity values ρ_2 within the dataset. In the above equation $T_{2,LM}$ is measured in s, $S_{por,BET}$ in um^{-1}. As ρ_2 has not been measured here we may infer ρ_2 from inserting (8) into (3) with q_p=1 leading to the TNMR variant of the Kozeny-Carman relation

$$K \cdot F = 137.39 \cdot T_{2,LM}^2 \quad (9)$$

with K measured in Darcy, and $T_{2,LM}$ in s. Comparing (9) to (1) implies ρ_2=5…25um/s, a range of values in accordance with those reported by Kleinberg [8].

APPLICATIONS

Relations (8) and (9) are the main results of this study. Applicability may be demonstrated by comparing (9) to standard permeability estimators used in the logging industry, namely those by Sen [9] and Timur-Coates [10]. Figure 7 indicates the simple relationships between these expressions and further implies that multiplier rules may be applied to transform between them. In a recently drilled Lublin Basin exploration well TNMR log derived permeability estimators subsequently calibrated by applying (9) compare favorably with both permeabilities inferred from wireline formation tests and those derived from log inversion and application of Herron's k-lambda permeability estimator [11] (fig.8). Here k-lambda values are based on a Kozeny-Carman type equation (1) with the S_{por} term computed from interpreted formation mineral volumes and may generally be regarded suitable for clay bearing sand interpretation.

Large deviations from (9) are to be expected when applied to porous systems with authigenic clay meshworks blocking hydraulic continuity across pore throats. In that case TNMR data may still be acquired in the fast diffusion limit and thus be related to specific

surface area of the bulk pores mainly. The additional clay meshwork surface area is not accounted for leading to underestimating the lamellar factor and therefore overestimating permeabilities by application of (9). This has been seen on a dataset acquired in a well offset from the Lublin Basin. TNMR derived permeabilities overestimated by more than one order of magnitude those derived from Stoneley wave dispersion and wireline formation test mobilities. Subsequently rotary sidewall cores were taken across the zone of interest. Laboratory air permeability measurements and thin section inspection confirmed the existence of pore throat blocking clay meshworks thus explaining the low permeability values measured across these samples.

CONCLUSIONS

Strong correlations were shown to exist between surface area estimates derived from nitrogen gas adsorption (BET), mercury intrusion capillary pressure (MICP), and transverse nuclear magnetic resonance measurements (TNMR) measured on vintage core plugs of Permian and Carboniferous age from the Lublin Basin, Poland. The physical significance of these correlations was facilitated by comparing results to a fractal void-solid interface model, the Pape pigeon hole model.

As a main result, surface scaling (8) and permeability estimators (9) based on TNMR well logs were derived.

TNMR logging may not be able to provide all input for a working permeability estimator, as shown above, and redundant estimators derived from logs based on dynamic measurements (sonic, formation tests) may still be needed. This redundancy is in fact necessary to identify facies types not represented in the core database and therefore may aid in the process of conditional sidewall core sampling, a procedure recently suggested by Worthington [12].

NOMENCLATURE

F	formation factor
K	permeability, $[K]=D=0.987 um^2$
Q_{ik}	conversion factor for inner surface area measurements with yardsticks i and k
$q0$	lamellar factor from the PARIS equation
r_{eff}	effective hydraulic radius in the Kozeny-Carman equation, $[r_{eff}]=um$
r_c	capillary radius corresponding to capillary pressure P_c, $[r_c]=um$
r_{min}	minimum capillary radius corresponding to maximum capillary pressure, $[r_{min}]=um$
S_{por}	specific surface area/pore surface-to-volume ratio, $[S_{por}]=m^2/cm^3=um^{-1}$
$T_{2,LM}$	log-mean transverse relaxation time, $[T_2]=s$

REFERENCES

[1] Basan, P., Lowden, B., Whattler, P., Attard, J., Pore-size data in petrophysics: a perspective on the measurement of pore geometry", *from* Lovell M., Harvey P. (eds), *Developments in Petrophysics*, Geological Society Publication No.122 (1997), 47-67.

[2] East, D., The use of surface area data obtained on reservoir core samples", *SCA Proceedings* (1998) CD ROM, SCA-9839.

[3] Volokitin, Y., Looyestijn, W., Slijkerman, F., Hofman, J., A practical approach to obtain primary drainage capillary pressure curves from NMR core and log data", *Petrophysics* (2001) **42**, 334-343.

[4] Pape, H., Riepe, L., Schopper, J., A pigeon-hole model for relating permeability to specific surface", *The Log Analyst* (1982) **23**, 5-13; Errata, *The Log Analyst* (1982) **23**, 50.

[5] Pape, H., Riepe, L., Schopper, J., Conversion between specific surface area measurements of different resolution power with the aid of pigeon-hole model theory", *from* Haynes J., Rossi-Diora P. (eds), *Principles and applications of pore structural characterization*, Arrowsmith, London (1985), 117-131.

[6] Brunnauer, S., Emmett, P., Teller, E., Adsorption of gases in multimolecular layers, *J. Am. Chem. Soc.* (1938) **60**, 309-319.

[7] Pape, H., Riepe, L., Schopper, J., Interlayer conductivity of rocks – a fractal model of interface irregularities for calculating interlayer conductivity of natural porous mineral systems", *Colloids and Surfaces* (1987) **27**, 97-122.

[8] Kleinberg, R., Utility of NMR T_2 distributions, connection with capillary pressure, clay effects, and determination of surface relaxivity parameter ρ_2", *Magnetic Resonance Imaging* (1996) **14**, 761-767.

[9] Sen, P., Straley, C., Kenyon, W., Whittingham, M., Surface to volume ratio, charge density, nuclear magnetic relaxation and permeability in clay bearing sandstones", *Geophysics* (1990) **55**(1), 61-69.

[10] Timur, A., Effective porosity and permeability of sandstones investigated through nuclear magnetic principles", *The Log Analyst* (1969) **10**, 3-11.

[11] Herron, M., Johnson, D., Schwartz, L., A robust permeability estimator for siliclastics", *SPE Proceedings* (1998) SPE 49301, 777-787.

[12] Worthington, P., A validation criterion to optimize core sampling for the characterization of petrophysical facies, *Petrophysics* (2002) **43**(6), 477-493.

[13] Pape, H., Clauser, C., Iffland, J., Permeability prediction for reservoir sandstones and basement rocks based on fractal pore space geometry", *Geophysics* (1999) **64**(5), 1447-1460.

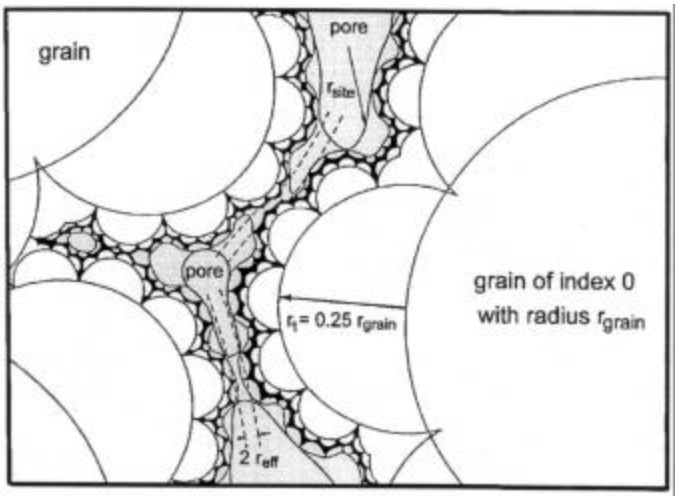

Figure 1. Cross-section of pore and grain system with composite convolution structures scaling with factor 0.25 or, equivalently, featuring surface structures with fractal Hausdorff dimension D_f=2.3566, adapted from [13].

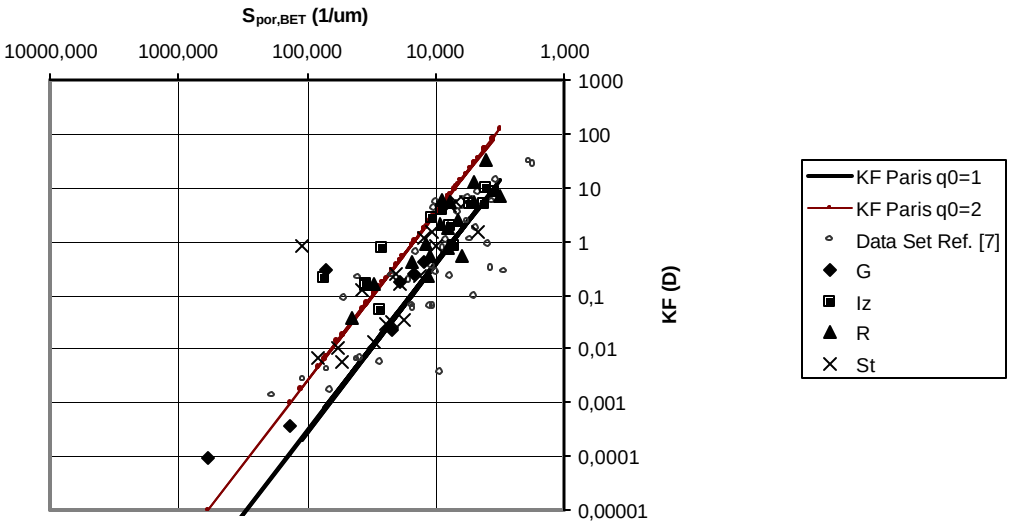

Figure 2. Product of air permeability K(D) and formation factor F plotted against specific inner surface area $S_{por,BET}$ using data from four Lublin Basin wells G, Iz, R, and St. Also shown trend lines from the PARIS equation (3) as explained in the main text and the dataset from reference [7] which has been used to derive the PARIS equation.

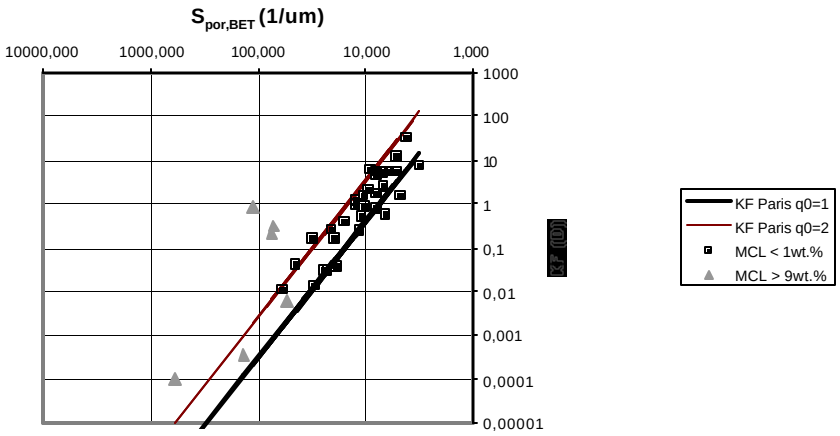

Figure 3. Same data from Lublin Basin as in figure 2, indexed by XRD clay content MCL. Samples with large detrital clay content plot in the bottom part of the figure and still follow the trend given by the PARIS equation for low q_0. Samples with large authigenic clay content plot to the left of the shown trend lines, constituting pore systems with large lamellar factors q_0>2.

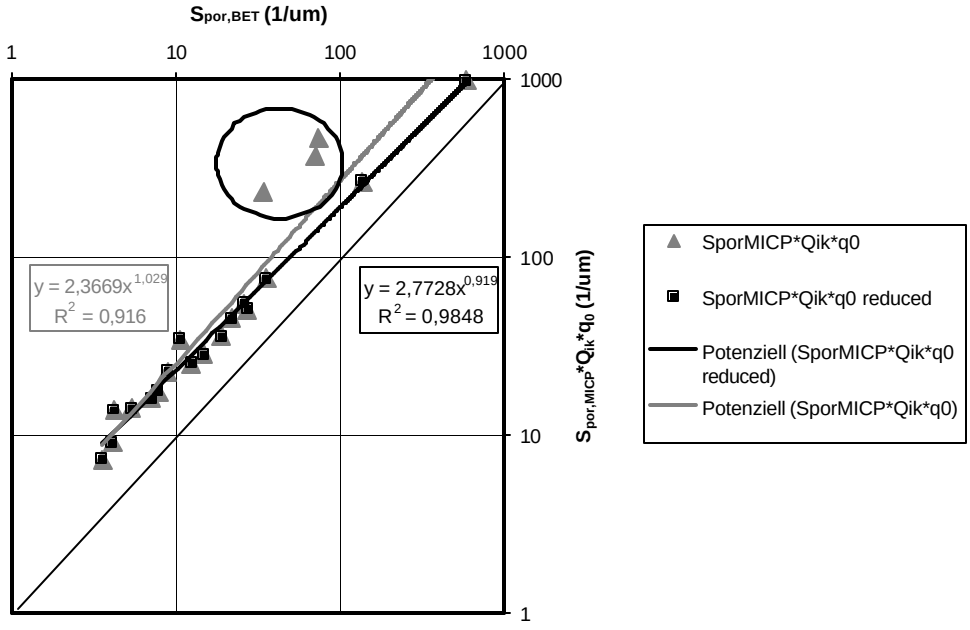

Figure 4. Conversion for MICP and BET based inner surface area measurements. All data points are generated using Q_{ik} from (6). Gray triangle data points are generated by converting with q_0 from (2), black square data points do not take into account samples with high capillary entry pressure (circled

data points) as depicted in figure 5. Combining both conversion methods leads to the balanced correlation (7) given in the main text.

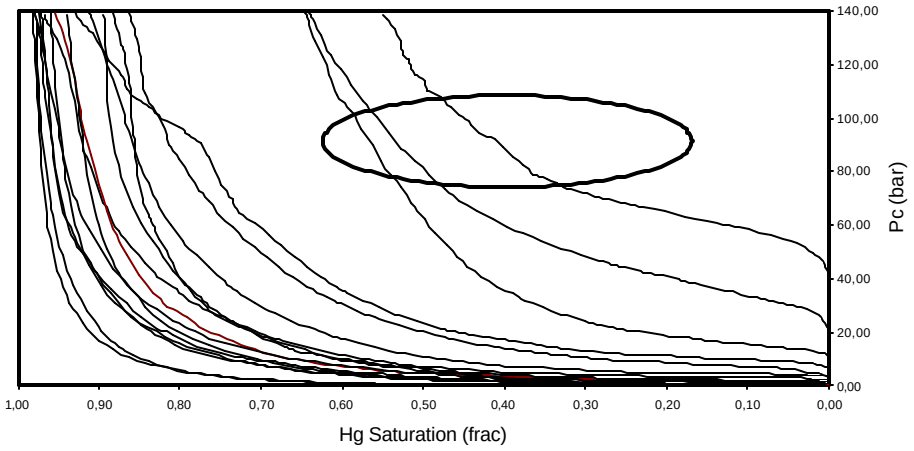

Figure 5. MICP functions for samples from the Lublin Basin database. Curves circled correspond to high capillary entry pressure samples which were partly disregarded from the MICP-BET surface area conversion.

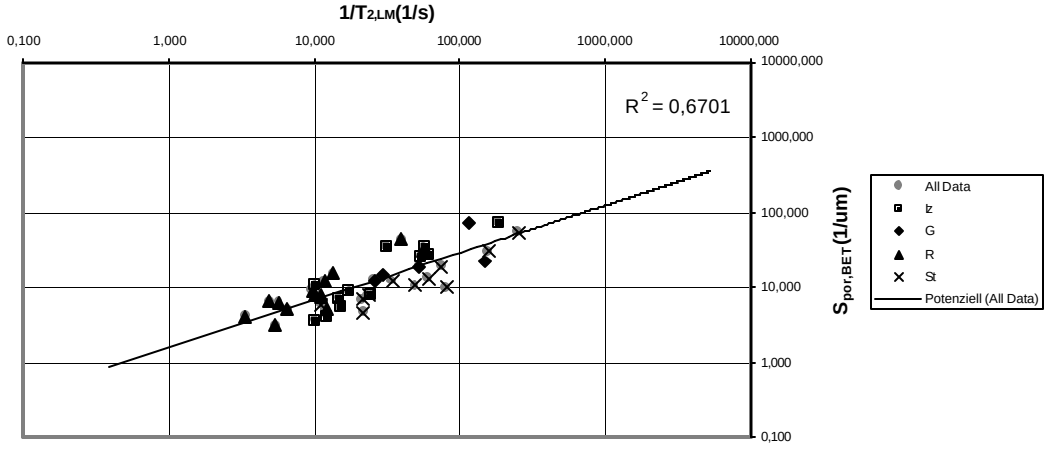

Figure 6. Conversion of TNMR log-mean T_2 times to BET based inner surface area measurements. Note the considerable scatter around the correlation line which may be attributed to the variability of surface relaxivity values r_2.

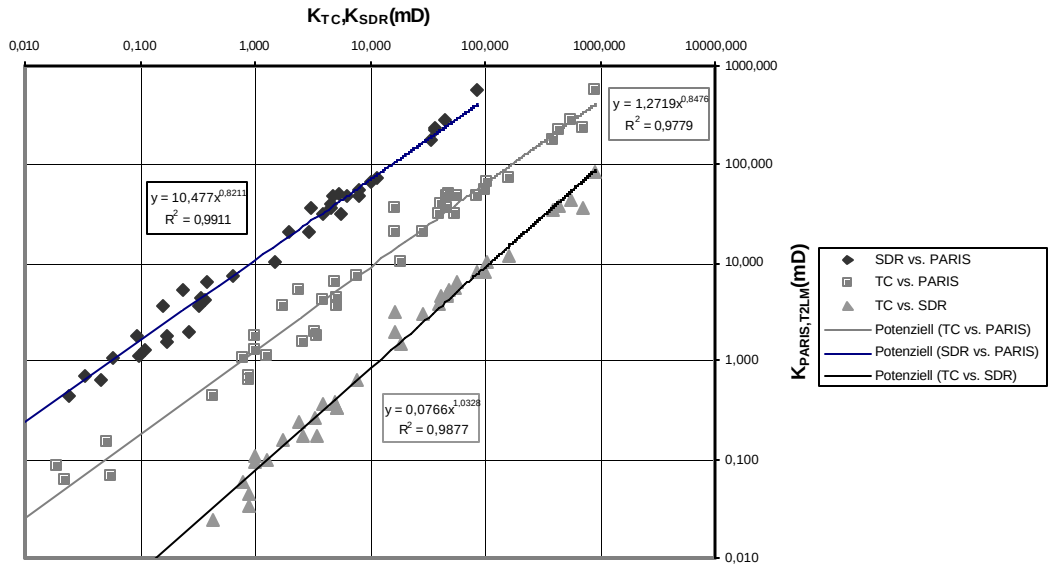

Figure 7. Correlation of T_{2LM} based PARIS permeability predictions $K_{PARIS,T2LM}$ with standard TNMR log based predictors from Timur-Coates K_{TC} and Sen K_{SDR}. Depicted log-log correlations allow for accurate transformation between the different permeability representations.

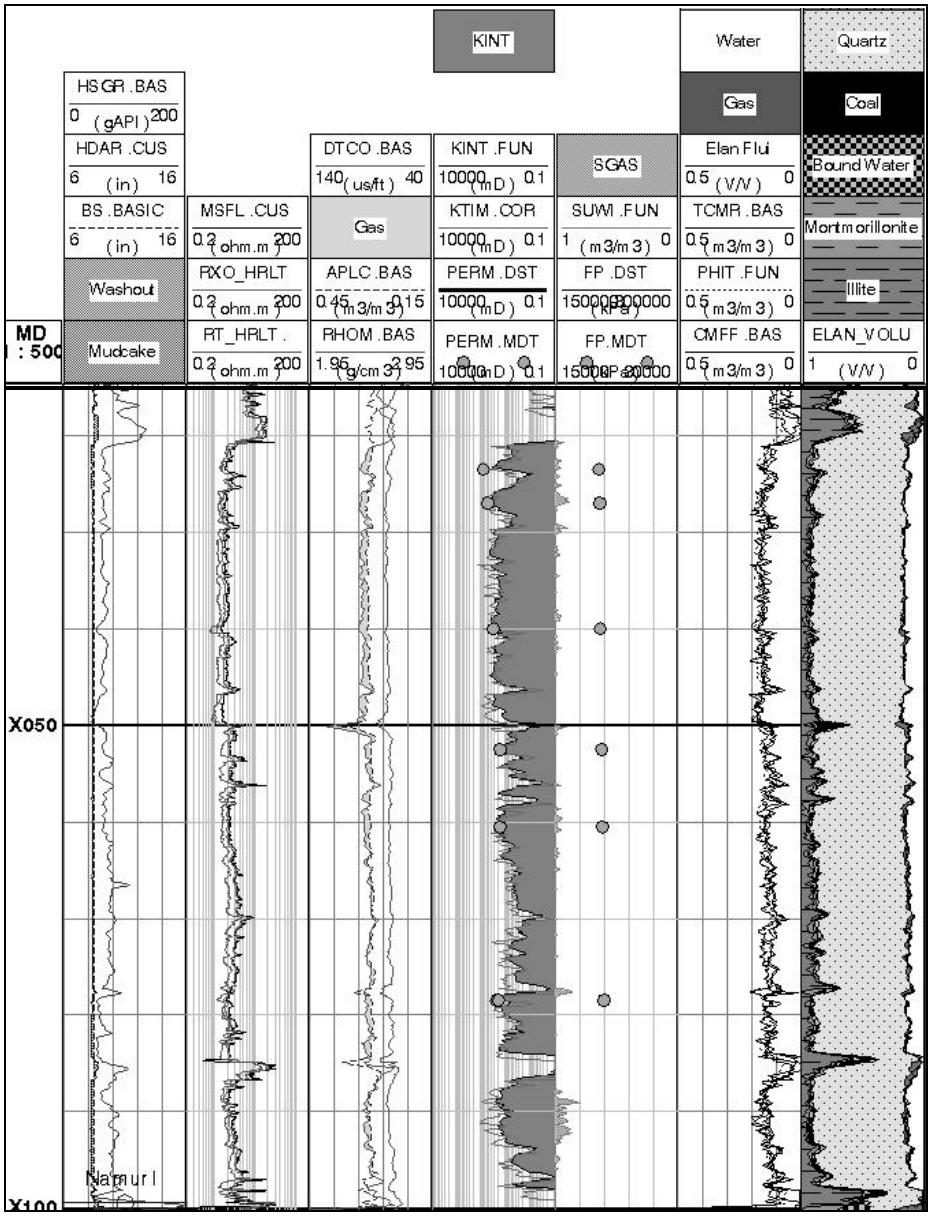

Figure 8. Log example from a newly drilled well in the Lublin Basin showing standard open hole logs in track 1 through 3, permeability estimators in track 4, water saturation and formation pressure in track 5, interpreted fluid and mineral volumes in track 6 and 7. Permeability estimators derived from formation volume interpretation (KINT, gray shading), calibrated TNMR log (KTIM) based on correlations from fig. 7, and wireline formation tester mobilities compare well in this water zone.